A Novel Tree Shrew (*Tupaia belangeri*) Model of Glaucoma

Brian C. Samuels,[1] John T. Siegwart,[2] Wenjie Zhan,[1] Lisa Hethcox,[1] Melissa Chimento,[3] Ryan Whitley,[1] J. Crawford Downs,[1] and Christopher A. Girkin[1]

[1]Department of Ophthalmology, University of Alabama at Birmingham School of Medicine, Birmingham, Alabama, United States
[2]Department of Vision Sciences, School of Optometry, University of Alabama at Birmingham, Birmingham, Alabama, United States
[3]High Resolution Imaging Facility, University of Alabama at Birmingham School of Medicine, Birmingham, Alabama, United States

Correspondence: Brian C. Samuels, University of Alabama at Birmingham, 1670 University Boulevard, Volker Hall Room B130, Birmingham, AL 35294, USA; bsamuels@uabmc.edu.

Submitted: March 3, 2018
Accepted: May 18, 2018

Citation: Samuels BC, Siegwart JT, Zhan W, et al. A novel tree shrew (*Tupaia belangeri*) model of glaucoma. *Invest Ophthalmol Vis Sci*. 2018;59:3136–3143. https://doi.org/10.1167/iovs.18-24261

Purpose. Primates and rodents are used widely as animal models of glaucoma, but each has significant limitations. Researchers need additional animal models that closely resemble the relevant anatomy and pathologic features of the human disease to more quickly advance research. We validate a novel glaucoma animal model in tree shrews (*Tupaia belangeri*).

Methods. Experimental glaucoma was induced in adult tree shrews ($n = 8$) by injecting 50 µL of a 25 mg/mL ferromagnetic bead solution into the anterior chamber. Beads were directed into the iridocorneal angle with a magnet to impede aqueous outflow. Animals were followed for 3 months with weekly IOP measurements and biweekly spectral domain optical coherence tomography (SD-OCT) images of the optic nerve head. Histopathology of the optic nerve and optic nerve axon counts were completed at the end of the study.

Results. The 12-week average mean IOP was 22.7 ± 3.6 and 8.6 ± 2.9 mm Hg in the treated and control eyes, respectively. Longitudinal analysis showed significant retinal nerve fiber layer (RNFL) thinning throughout the study. Axon counts were significantly reduced (59.7%) in treated versus control eyes. SD-OCT imaging showed cupping and posterior displacement of the lamina cribrosa in glaucomatous eyes. RNFL thickness and optic nerve axon counts were reduced consistent with IOP elevation. Optic nerves demonstrated histopathology consistent with glaucomatous optic neuropathy.

Conclusions. Tree shrews with experimental glaucoma show key pathologic characteristics of the human disease. The tree shrew model of glaucoma has the potential to help researchers accelerate our understanding of glaucoma pathophysiology.

Keywords: glaucoma, tree shrew, intraocular pressure, retinal ganglion cells, lamina cribrosa

Glaucoma is a leading cause of blindness worldwide,[1,2] yet we still are trying to develop a fundamental understanding of the underlying pathophysiologic mechanisms that lead to retinal ganglion cell (RGC) death. Development of animal models that accurately reflect the pathophysiology of human diseases is critical to advancing our understanding of the disease pathogenesis and its progression. Moreover, these models are instrumental in helping translate basic science discoveries, such as novel pharmacologic therapeutics, from in vitro, preclinical stages into human clinical trials.

The preponderance of evidence strongly suggests that the RGC axonal injury occurring within the lamina cribrosa is a critical component of glaucomatous injury.[3–9] This has led to increasing interest in understanding the mechanobiology of the optic nerve head (ONH) and the role of translaminar pressure differences in the development and progression of glaucoma. To understand these relationships, researchers must use animal models that most closely resemble the relevant human anatomy and develop key pathologic features of the human disease.

While nonhuman primates represent the most ideal animal model for certain types of glaucoma research due to their complex load-bearing collagenous lamina cribrosa resembling humans,[10–13] these models are costly and, thus, not applicable to larger studies required to evaluate new treatments. Alternatively, many researchers have chosen to use rat[14–20] or mouse[21–24] models of glaucoma in their research. Murine models have the advantage of allowing unparalleled study of the genetic and molecular pathobiology underlying glaucoma.[25–29] However, similar to rat models, mice lack a well-developed load-bearing ONH lamina cribrosa.[30,31] This structure is critical for investigating many of the biomechanical aspects of glaucoma, including, most critically, remodeling of the load-bearing connective tissues. In contrast, the tree shrew (*Tupaia belangeri*) is a small mammal closely related to primates[32] that currently is used in vision research as an inducible myopia model.[33,34] Tree shrews are accessible and, most importantly, have a robust connective tissue lamina with horizontally-oriented laminar beams that insert into the peripapillary sclera and, thus, are load-bearing.[35] We validated a novel animal model of glaucoma in tree shrews by demonstrating a reliable method to chronically elevate IOP with resultant selective gradual loss of the RGC and retinal nerve fiber (RNFL) layers, histopathologic evidence of glaucomatous optic neuropathy, and remodeling of the load-bearing connective tissues of the ONHs consistent with human glaucoma.

Methods

Animal Preparation

All procedures were performed in compliance with the Association for Research in Vision and Ophthalmology Statement on the Use of Animals in Ophthalmic and Vision Research

Figure 1. The right eye of a tree shrew (*T. belangeri*) immediately following injection of ferromagnetic beads into the anterior chamber. Beads are evenly distributed in the iridocorneal angle (*orange ring* at the *arrow tips*) at the junction of the iris and a clear cornea.

and were approved by the University of Alabama at Birmingham's Institutional Animal Care and Use Committee. Adult male and female tree shrews ($n = 8$) ranging from 1.7 to 7.7 years old (mean, 5.0 years) were used in this study. Animals were housed individually on a 12-hour light–dark cycle (lights on at 7:00 AM) with access to food and water ad libitum. For all procedures (induction of ocular hypertension, IOP measurements, and optical coherence tomography [OCT] imaging), animals were transported to the procedure rooms in their individual nest boxes. At the end of each procedure, animals were returned to their nest boxes and observed until fully mobile, at which point they were returned to their home cages. During the recovery period, nest boxes were warmed using a heating blanket.

Ferro-Magnetic Bead Preparation

A modified version of the technique of Samsel et al.[36] for induction of ocular hypertension was used. Ferromagnetic microspheres measuring 10 μm in diameter (Cat#109319-10; Corpuscular, Inc., Cold Spring, NY, USA) required thorough washing to prohibit a uveitic response after injection into the anterior chamber. The microspheres were resuspended via vortex mixer and aliquots placed into 1 mL centrifuge tubes. Microspheres then were spun down at 5400*g* for 2 minutes. The supernatant was removed and beads were resuspended in sterile balanced salt solution (BSS) using the vortex mixer. This process was repeated three times.

Induction of Ocular Hypertension

Isoflurane anesthesia was induced (3.0%–4.0% isoflurane at an O_2 flow of 2.0 L/min) by connecting the small animal anesthesia machine (Summit Medical Equipment, Bend, OR, USA) directly to the nest box. Once anesthesia was accomplished, animals were placed on a sterile surgical field under an operating microscope. Body temperature was maintained at 37°C throughout the experiment via a homeothermic blanket (Harvard Apparatus, Holliston, MA, USA). Topical proparacaine 0.5% was placed in the eye as supplemental anesthesia. The eyelids were washed three times with 5% betadine and one drop of betadine was instilled into the eye. Sterile BSS was used to rinse the eyelids and eye preoperatively. Under microscopic visualization, the anterior chamber was cannulated with a 30-gauge needle on a tuberculin syringe and 50 μL ferromagnetic microspheres at a concentration of 25 mg/mL were injected into the anterior chamber. The 30-gauge needle could be rotated slightly in the iris plane to allow leakage of aqueous humor through the paracentesis to avoid an acute, high elevation of IOP immediately following microsphere injection and angle occlusion. Following injection, a neodymium magnet was used to guide and evenly relocate the beads 360° throughout the angle (Fig. 1). Bacitracin ophthalmic ointment was placed in the operative eye and the animal was returned to the nest box for recovery.

IOP Measurement

IOP was monitored throughout the experiment using the Icare TonoLab rebound tonometer (Icare Finland Oy, Helsinki, Finland). The Icare TonoLab is factory calibrated with standard settings for mice and rats. We previously had performed a calibration of this TonoLab rebound tonometer for isoflurane-anesthetized tree shrews, and this standardization curve was used to calculate the IOP readings throughout the current experiments. IOPs were recorded for 14 consecutive weeks, starting 1 week before and ending 12 weeks after magnetic microsphere injection. Animals were placed under isoflurane anesthesia as described previously. Immediately upon induction, animals were placed on an elevated platform that supported the head and body to allow easy access to both eyes for IOP measurements. Care was taken to ensure the tonometer bore remained in the horizontal position and all measures were taken from the center of the cornea. All IOPs were taken 10 times and averaged for each time point.

Spectral Domain Optical Coherence Tomography (SD-OCT) Imaging

Baseline in vivo SD-OCT imaging was performed 1 week before microsphere injection and biweekly for 12 weeks following each IOP assessment using the Spectralis SD-OCT (Heidelberg Engineering, Inc., Heidelberg, Germany). One drop 1% tropicamide and 2.5% phenylephrine was used to dilate the iris. A 20° × 15° raster scan through the ONH consisting of 37 high-resolution line B-Scans (9 scans/line averaged under ART Eye Tracking) in Enhanced Depth Imaging (EDI) mode, a 20° radial scan through the ONH consisting of 24 high-resolution B-Scans (18 scans/line averaged under ART Eye Tracking) in EDI mode, and the peripapillary RNFL thickness were measured using a circle scan at each time point. OCT images were analyzed for changes in peripapillary RNFL thickness, and the ONH line B-scans delineated for comparison to ONH sagittal reconstructions. All ONH images were exported in RAW (.vol) format and opened with the open source image processing program Fiji (ImageJ; National Institutes of Health [NIH],

Investigative Ophthalmology & Visual Science

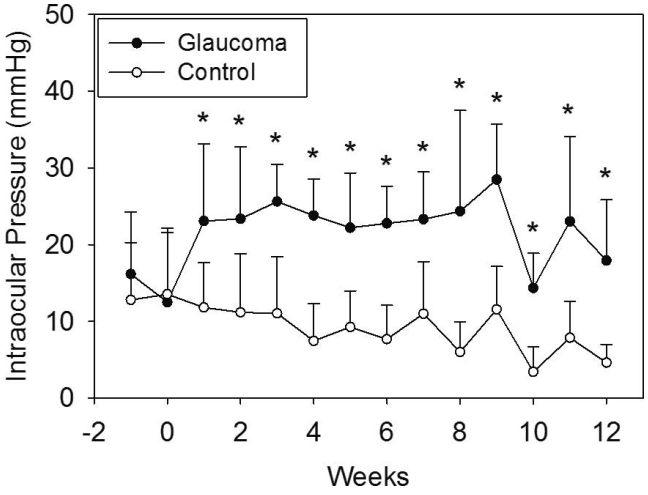

Figure 2. Plot of the mean ± SD of IOP in the tree shrews' treated and control eyes. Time 0 is the day of bead injection. IOPs were similar between treatment groups at baseline ($P = 0.43$ and 0.82 at 1 week before and on the day of microinjections, respectively). There was an IOP versus time effect (repeated measures ANOVA, $P < 0.001$) and IOP was significantly elevated in the treated eye at every time point following treatment. (*$P = 0.021$ at week after injection and $P < 0.01$ at all other time points).

Bethesda, MD, USA) using the Open Heyex Raw plugin. Gamma then was adjusted to 0.35 and contrast enhanced 0.1%.

Tissue Collection and Histopathologic Analysis

At the end of the study, all animals were deeply anesthetized with xylazine (50 mg intraperitoneally [IP]). The anterior chamber of each eye was cannulated with a 30-gauge needle attached to a reservoir of PBS for control of IOP during fixation. Glaucomatous eyes were pressurized to the 6-month mean IOP, while the fellow control eyes were pressurized to the normal baseline IOP. The animals were perfused transcardially with 180 mL of PBS followed by 180 mL 4% paraformaldehyde. The brain, optic nerves, and eyes were explanted in toto. The eyes will be used for histomorphometric analysis and 3-dimensional (3D) reconstruction in a future study.

Optic nerves were collected for automated, 100% optic nerve axon counts using AxonMaster software in a manner similar to that of Reynaud et al.[37] Briefly, optic nerves were resin-embedded using an EMBED-812 embedding kit (Electron Microscopy Sciences, Hatfield, PA, USA), and 1-μm cross-sections were stained for myelin using *P*-phenylenediamine (1,4 D diamine benzene *P*-phenylenediamine; PPD) as follows: A 2% solution of PPD stain (Sigma Aldrich Corp., St. Louis, MO, USA) was created in 50% ethanol. The PPD stain was kept in a foil-wrapped, dark glass jar with a tight paraffin lined lid to protect it from light and prevent the ethanol from evaporating. PPD stain was filtered with a 0.2 μm nylon sterile filter before use. Slides containing optic nerve sections were stained at room temperature for approximately 20 minutes (time was adjusted slightly to obtain consistency in the desired staining intensity with each batch of slides). Once staining was complete, slides were rinsed in 100% 2-propanol and allowed to dry on a warming plate. Slides then were coverslipped and allowed to dry before imaging. The entire nerve cross-section was imaged and montaged at ×100 using an Olympus VS120 robotic microscope on a BX61 platform that was equipped with an automated slide scanner and CellSens (Olympus Corp., Tokyo, Japan) control software. In addition to axon counts, retrobulbar optic nerve sections were examined under bright field microscopy to determine the severity of glaucomatous optic neuropathy by histopathologic analysis.

Table 1. IOPs of Control and Treated Eyes Throughout the Study Period

Week	Treated	Control	*P* Value
−1	16.2 ± 8.1	12.8 ± 7.5	0.44
0	12.5 ± 9.1	13.5 ± 8.6	0.83
1	23.1 ± 10.1	11.8 ± 5.9	0.021*
2	23.4 ± 9.4	11.2 ± 7.7	0.005*
3	25.6 ± 4.9	11.0 ± 7.4	<0.001*
4	23.8 ± 4.8	7.4 ± 4.9	<0.001*
5	22.2 ± 7.1	9.3 ± 4.7	<0.001*
6	22.8 ± 4.9	7.7 ± 4.4	<0.001*
7	23.3 ± 6.2	11.0 ± 6.8	<0.001*
8	24.4 ± 13.1	6.0 ± 3.9	0.001*
9	28.5 ± 7.2	11.6 ± 5.6	0.001*
10	14.3 ± 4.5	3.4 ± 3.3	<0.001*
11	23.1 ± 11.1	7.9 ± 4.8	0.001*
12	17.9 ± 7.9	4.6 ± 2.4	<0.001*

* $P < 0.05$.

Statistical Analysis

Baseline IOP and RNFL values between the magnetic microsphere injected and control eye were compared using an independent *t*-test. A repeated measures ANOVA then was used to determine whether microinjection of magnetic microspheres into the anterior chamber angle had a treatment-by-time effect on IOP and RNFL thickness. Where a time effect was found, an unpaired, 2-tailed *t*-test was used to compare individual time points between the treated and control groups. Total axon counts between the treated and control groups were compared using an independent 2-tailed *t*-test. All data are reported as mean ± SD. Significance was considered $P < 0.05$ for all experiments.

Similar to rodents, there is interanimal variability in the number of optic nerve axons. In studies comparing optic nerve axon counts to accumulated IOP (IOP × Days) and RNFL thickness, we normalized the axons counts by determining the percent of axons remaining in the experimental compared to the control eyes. Linear regression analysis was used to compare normalized 100% optic nerve axon counts versus accumulated IOP and versus change from baseline RNFL thickness.

Results

Injection of ferromagnetic beads resulted in sustained IOP elevation for the duration of the study at all time points compared to the control eye (Fig. 2, Table 1) while maintaining optical clarity of the lens and cornea needed for funduscopic examination and imaging. The range of IOP elevation following microbead injection was 14.3 ± 4.5 to 28.5 ± 7.2 mm Hg over the 12-week follow-up in the treated eyes. Mean IOP in the treated eyes was significantly elevated compared to the control eyes (average 22.7 ± 3.6 and 8.6 ± 2.9 mm Hg, respectively) at all time points throughout the 12-week follow-up period (Table 1). The individual means and standard deviation are illustrated in Table 1 and Figure 2.

The results of RNFL thickness obtained at baseline and throughout the 12-week follow-up are shown in Table 2 and Figure 3. There was a significant reduction in RNFL thickness at 2 weeks following IOP elevation, with a continual gradual decline in RNFL thickness throughout the duration of the study

Investigative Ophthalmology & Visual Science

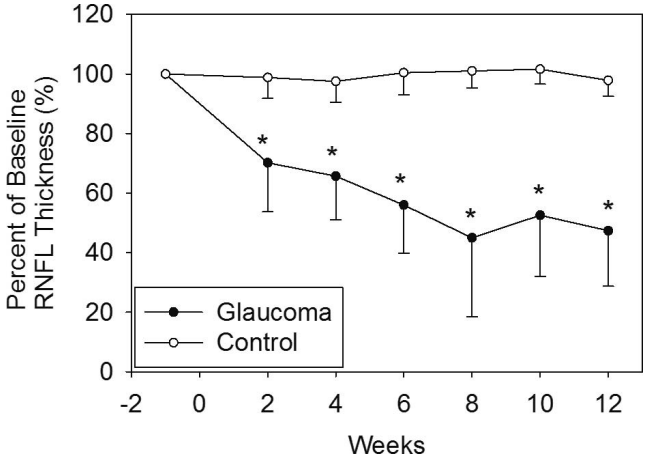

FIGURE 3. Plot of the change in RNFL thickness compared to baseline during follow-up. Measures were taken every 2 weeks. There was an RNFL versus time effect (repeated measures ANOVA. $P < 0.001$). Differences between treated and control eyes were significant at all time points after treatment ($P < 0.001$ at all time points).

as determined by repeated measures ANOVA ($P < 0.001$). The treated eyes showed significantly thinner RNFL compared to control eyes at all time points following IOP elevation (Table 2). Furthermore, the amount of RNFL reduction was related to duration and magnitude of IOP elevation (IOP*Days; Fig. 4).

There was a significant reduction in axonal number between treated and control eyes (112,676 ± 70,955 vs. 305,326 ± 100,560 axons, respectively; $P = 0.001$; Fig. 5). The extent of axonal loss, while highly variable, was negatively correlated with the magnitude and direction of IOP elevation (Fig. 4), but this correlation did not reach statistical significance ($r = 0.55$, $r^2 = 0.30$, $P = 0.16$). There also was a significant association ($r = 0.73$, $r^2 = 0.54$, $P = 0.038$) between RNFL loss (i.e., thickness of RNFL at the final examination compared to baseline) and axonal loss (Fig. 6).

Changes in the morphometry of the load-bearing connective tissues can be visualized in vivo using SD-OCT imaging. Figure 7 illustrates the progressive bowing of the lamina

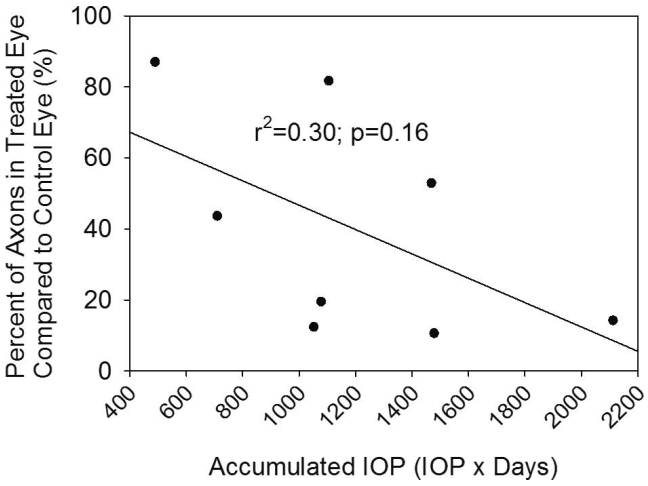

FIGURE 4. Plot of final RNFL thickness compared to baseline versus accumulated IOP (IOP × Days) for all eight animals. While there is some variability, there is a relationship between loss of RNFL and magnitude and duration of IOP elevation (IOP × Days) indicating that longer duration and magnitude of IOP elevation leads to increased RNFL loss.

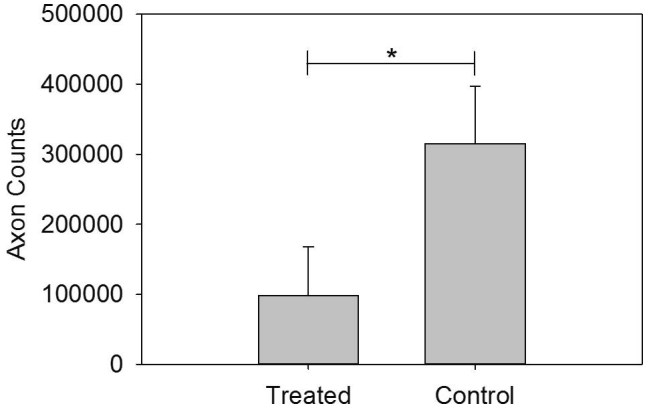

FIGURE 5. Means ± SD of total optic nerve axon counts across treatment and control groups. *$P = 0.001$.

cribrosa and posterior displacement of the anterior laminar surface in animals with increasing severity of experimental glaucoma compared to the normal control eyes. The post-processed OCT B-scans show a BMO plane to anterior laminar surface distance in the normal, mild glaucoma, and severe glaucoma animals of 3, 15, and 27 pixels, respectively. Due to the optical magnification caused by the tree shrew's eye, the pixel-to-micrometer conversion on the Spectralis SD-OCT is not valid for this species. We are currently working on validation studies to determine the appropriate pixel-to-micrometer conversion factor for the tree shrew that will allow more objective measures in the future.

DISCUSSION

Our study demonstrated that injection of ferromagnetic beads into the anterior chamber of the tree shrew can generate a sustained elevation of IOP that results in damage to the optic nerve consistent with glaucomatous injury seen in human disease. In vivo, longitudinal observation with SD-OCT showed gradual reduction in RNFL thickness, while the outer retinal layers were preserved. In addition, examination of the retrobulbar portion of the optic nerve demonstrated an optic neuropathy characterized by reduction in total axonal number and axon density (Fig. 8), similar to the human condition.

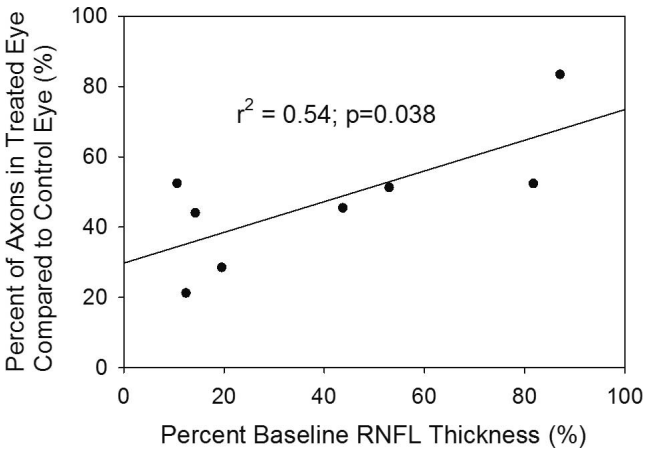

FIGURE 6. Scatter plot of the association between the final RNFL thickness compared to baseline versus the axon count of the injected eye compared to the fellow eye at the end of follow-up. The final RNFL thickness and axon counts are highly correlated.

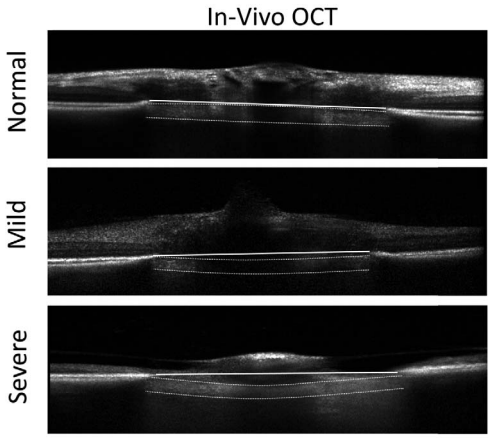

FIGURE 7. OCT b-scans through the tree shrew ONH comparing a normal control eye (*top*) to eyes with mild (*middle*) and severe (*bottom*) glaucomatous damage. The *horizontal white line* represents the Bruchs' membrane opening (BMO) plane. The anterior and posterior surfaces of the lamina are clearly visible on OCT (see normal control eye as an unmarked example). In a normal animal, the anterior surface of the lamina cribrosa is located at or slightly above the BMO plane. The laminar surfaces are delineated by the *white dashed lines* in the glaucomatous animals for comparison. The lamina bows and is displaced progressively further posterior with increasing severity.

Tree shrews appear to offer researchers several advantages as a small animal model for glaucoma. All species of tree shrews share several common features, including omnivorous diet, a skeleton that is in an unspecialized mammalian pattern, small body mass, nonprehensile feet, claws on all digits, and a large brain-to-body mass ratio. There has been some controversy in the past as to the correct phylogenetic classification of the tree shrew. Similarities in brain and eye anatomy among other internal characteristics led to the initial classification of the tree shrew as a primitive primate. Genetic analysis does show that the tree shrew is in proximity to primates,[38] and they have been used widely as an alternative model to higher primates for studies of psychosocial stress,[39] hepatitis,[40] and myopia.[33,34] However, tree shrews do not appear to share any derived characteristics. Thus, they are now classified independently in the order Scandentia.[38] Because the tree shrew ocular anatomy is closer to primates than rodents, the tree shrew model bridges a gap between established rodent and primate models of glaucoma.

The method used to elevate pressure in tree shrews is a modified approach similar to that described by Samsel et al.[36] for induction of glaucoma in other rodent models that use ferromagnetic microspheres. The advantage of this technique is that the beads occlude the trabecular meshwork while allowing visualization of the posterior segment by preserving the clarity of the ocular media. This approach was chosen after several other methods that have been used in other mammalian animal models were tried with limited success. These prior unsuccessful approaches included: (1) 360° laser photoablation of the trabecular meshwork, (2) hypertonic saline injection into the episcleral veins, (3) thermal cautery of the episcleral veins, and (4) latex bead injection into the anterior chamber. A large iris root vessel mostly obscures the trabecular meshwork in the tree shrew and makes complete laser application impossible. Hypertonic saline and thermal cautery did not elevate IOP reliably, and microinjection of latex microspheres resulted in an inconsistent IOP elevation and frequently impaired the view to the posterior segment.

While there was a correlation between axonal loss and total accumulated IOP ($r = 0.55$, $r^2 = 0.30$, $P = 0.16$), this association

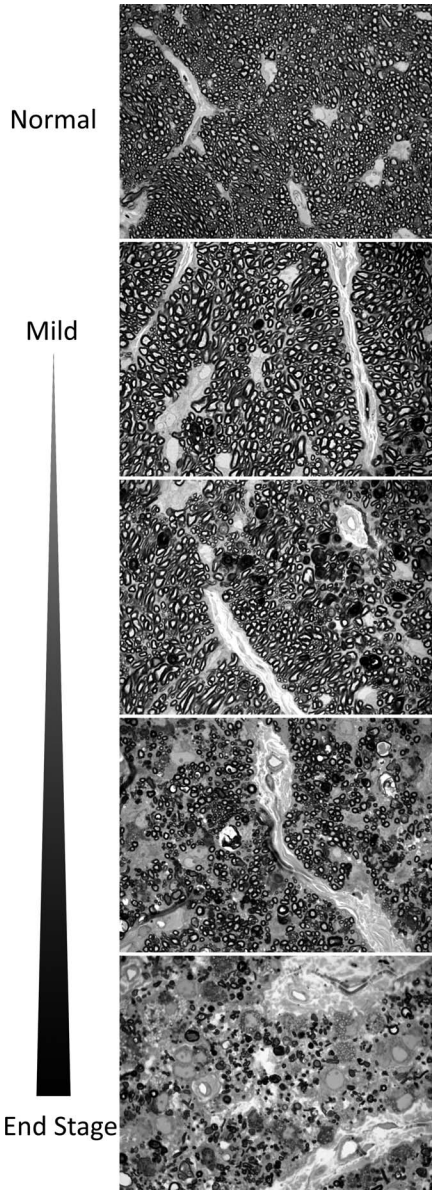

FIGURE 8. Axonal injury seen in treated eyes following microbead injection and IOP elevation showing wide variability in axonal injury from mild to extensive axonal loss. *Scale bar*: 25 μm.

was highly variable and did not reach significance. For example, for the five eyes that experienced more than 1000 IOP*days, the range of axonal loss varied from 18.2% to 89.4%. Part of this variability may be accentuated by the use of weekly IOP measurements in this study and may be minimized in the future by increasing the IOP measurement frequency. Notwithstanding, the variability in susceptibility to IOP-related injury seen in this study is similar to that of other small animal models[24,41] and may reflect individual differences in susceptibility to IOP-related injury that have been observed in human disease. The entire cohort showed a broad range of histopathologic injury (Fig. 8). Thus, this model can afford the opportunity to explore the characteristics associated with disease susceptibly.

The tree shrew model of glaucoma provides the opportunity to study changes in the optic nerve, retina, and central nervous system at various disease stages defined by structural loss in the retina and neuroretinal rim or remodeling changes

Investigative Ophthalmology & Visual Science

within the lamina cribrosa in vivo, as has been performed in models of glaucoma in higher primates.[42,43] Because the ferromagnetic beads can be drawn away from the pupil and visual axis, the current model allows for visualization of the posterior segment with SD-OCT imaging of the optic nerve and retina. This permits in vivo quantification of changes in these structures. These results clearly showed a time-dependent progressive thinning of the RNFL in response to increased IOP in the treated eye. Moreover, changes within the lamina cribrosa consistent with posterior deformation and remodeling potentially can be observed in these eyes. Figure 7 demonstrates representative changes seen in the ONH in an eye with early and more advanced damage. During the completion of this study, we began to recognize the potential for an even greater detailed analysis of the morphologic structures in the tree shrew ONH. With proper focus, post-image processing, and b-scan alignment, it is possible to identify individual laminar beams using higher raster volume scans (Fig. 9). All of our forthcoming studies will incorporate high raster volume scans through the ONH. Future studies also will be aimed at quantifying the remodeling occurring within the tree shrew lamina in more detail.

While other small animal models in the mouse[24] and rat[41] have demonstrated RGC loss and axonal injury at the level of the ONH, these animal models do not have load-bearing connective tissue trabeculae that span the neural canal. While mouse and rodent models are reasonable platforms in which to study axonal and retinal injury due to IOP elevation, they cannot be used to evaluate changes within the load-bearing connective tissue of the ONH. In contrast to other small animal models, changes in the structure of the load-bearing lamina cribrosa can be observed in tree shrews; thus, providing the opportunity to study the structural, cellular, and molecular changes in true load-bearing laminar beams.[35] The tree shrew model may be uniquely useful in experiments aimed at elucidating the molecular and cellular changes in the lamina cribrosa that occur in glaucoma.

Albon et al.[35] described the connective tissue architecture of the lamina cribrosa of the tree shrew and changes associated with aging. Their work revealed important similarities to the human lamina cribrosa, suggesting that it would make an excellent glaucoma model to study mechanobiology of the load-bearing connective tissue elements of the ONH. They demonstrated that the tree shrew optic nerve consists of a retrolaminar region consisting of vertically-oriented connective tissue septa and myelinated axons, a prelaminar region, and a laminar region with a similar microstructure to the human ONH in that the neural canal in this region is spanned by several fenestrated multilayer connective tissue 3D structures. These plates are composed of collagen types I, III, IV, V, and VI, fibronectin, and elastin in a similar fashion to that seen in the human. Moreover, these components also demonstrated changes with aging consistent with what has been shown in human disease. Thus, the tree shrew may make an excellent model to study the effects of aging, a primary risk factor or open-angle glaucoma (OAG), on vulnerability to IOP-related injury. Immunofluorescent labeling also demonstrated high levels of glial fibrillary acidic protein (GFAP) staining cellular process in the lamina cribrosa of the tree shrew suggesting the dense network of supportive astrocytes associates with these load-bearing connective tissue sheets.[35] These findings are again similar to that seen in the human lamina cribrosa and, hence, tree shrews provide a potential platform to study the effects of ONH mechanical strain and glaucomatous injury on cellular behavior within the lamina cribrosa using a small animal model. Lastly, the tree shrew also has three classes of RGCs, analogous to the W-, X-, and Y- cells in the cat, that have a variety of sizes and distributions within the lamina cribrosa.[44] Thus the model also could be used to examine vulnerability to individual subtypes of RGCs to IOP-induced changes within the microenvironment of the lamina cribrosa.

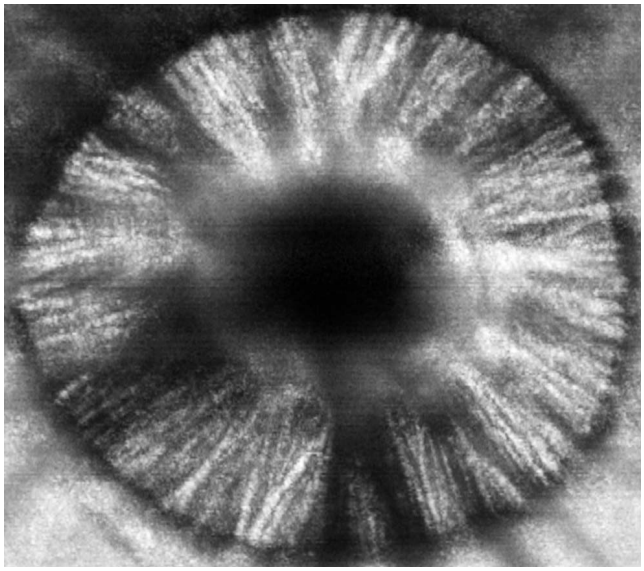

Figure 9. An en face reconstruction from a 391 raster volume scan through the ONH of the tree shrew at the level of the lamina cribrosa demonstrates the ability to identify individual laminar beams.

While this study has demonstrated the ability of this model to produce a "glaucoma-like injury," the study has some limitations. All animals were given similar volumes of magnetic beads and dispersed in a similar fashion throughout the angle, resulting in a fairly rapid loss of RNFL thickness due to IOP elevation. Future studies aimed at partially occluding the angle are planned to determine optimal titration of IOP elevation for a more gradual axonal injury to allow for evaluation of more chronic remodeling processes in the ONH. IOP was measured at several time points and did correlate with the degree of glaucomatous injury (axonal loss and decreased RNFL thickness). However, similar to all animal models and human disease, IOP is highly variable and true IOP exposure is not known. Future studies using implantable telemetric IOP sensors are planned to enhance the precision of the model. While the tree shrew has a similar load-bearing connective tissue lamina cribrosa compared to the human ONH, there are significant differences in the morphology of these tissues with a more radial orientation of load-bearing beams within the tree

Table 2. Percent of Baseline RNFL in Treated and Control Eyes Throughout the Study Period

Week	−1	2	4	6	8	10	12
Treated	100.0 ± 0.0	70.2 ± 16.4	65.7 ± 14.6	56.0 ± 16.1	45.0 ± 26.4	52.6 ± 20.6	47.4 ± 18.6
Control	100.0 ± 0.0	98.8 ± 7.0	97.5 ± 7.0	100.4 ± 7.3	101.0 ± 5.6	101.6 ± 5.0	97.8 ± 5.4
P value	–	<0.001*	0.001*	<0.001*	<0.001*	<0.001*	<0.001*

* $P < 0.05$.

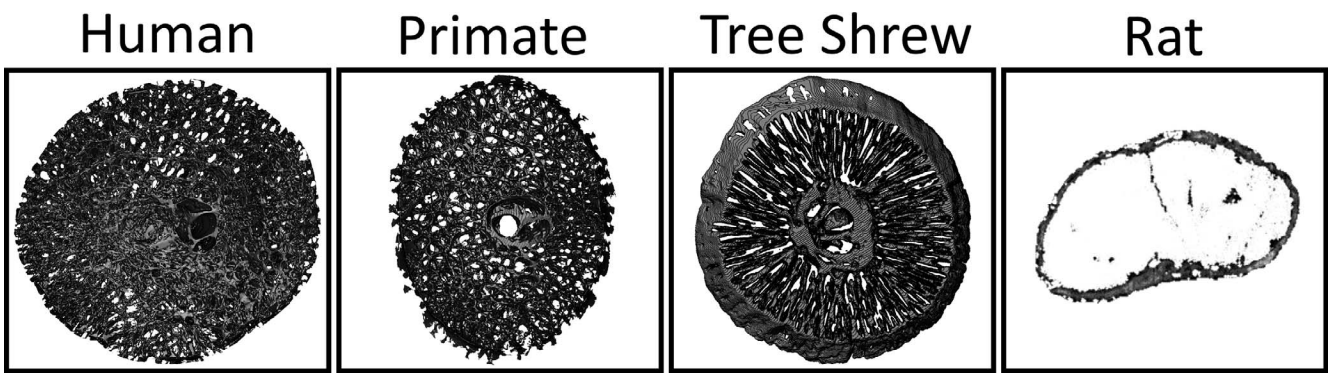

Figure 10. ONHs of a human, primate, and tree shrew were reconstructed using a serial sectioning and fluorescent episcopic imaging technique as described previously.[45,46] The collagenous connective tissues were segmented,[47] showing the trabeculated laminar microstructure in humans, nonhuman primates, and tree shrews, in contrast with rodents that lack a collagenous laminar structure.

shrew ONH (Fig. 10). However, given similar molecular and cellular characteristics, the tree shrew should be a better model to study the effects of laminar beam strain and the cellular and molecular components of the load-bearing beams within the ONH than existing small animal models that lack a collagenous load-bearing lamina.[35]

In summary, our study demonstrated that sustained moderate IOP elevation can be obtained using injection of ferromagnetic microbeads into the anterior chamber of the tree shrew. This results in a gradual reduction in RNFL thickness measured in vivo and significant axonal loss measured ex vivo. These changes are associated with a posterior remodeling of the lamina cribrosa that can be visualized in vivo using SD-OCT. The tree shrew glaucoma model has the potential to provide a less costly platform to study how alteration and variation in the load-bearing ONH connective tissues modulate glaucomatous injury. Moreover, given the extensive use of the tree shrew as a model of myopia, this model can be used to study the complex interaction between remodeling of the sclera and ONH seen in myopia and glaucoma.

Acknowledgments

The authors thank Thomas Norton, PhD, for his assistance in the early discussions on the development of this model as well as sharing his expertise in the use of tree shrews to model ophthalmic disease; and Jeff Messinger, BS, DC, for his assistance with aspects of the immunohistochemistry.

Supported in part by National Institutes of Health Grant R21EY026218 (BCS), the Glaucoma Research Foundation (CAG), the Eyesight Foundation of Alabama (CAG), and an unrestricted grant from Research to Prevent Blindness (CAG).

Disclosure: **B.C. Samuels**, None; **J.T. Siegwart**, None; **W. Zhan**, None; **L. Hethcox**, None; **M. Chimento**, None; **R. Whitley**, None; **J.C. Downs**, None; **C.A. Girkin**, None

References

1. Quigley HA, Broman AT. The number of people with glaucoma worldwide in 2010 and 2020. *Br J Ophthalmol*. 2006;90:262–267.
2. Friedman DS, Wolfs RC, O'Colmain BJ, et al. Prevalence of open-angle glaucoma among adults in the United States. *Arch Ophthalmol*. 2004;122:532–538.
3. Burgoyne CF, Downs JC, Bellezza AJ, Suh JK, Hart RT. The optic nerve head as a biomechanical structure: a new paradigm for understanding the role of IOP-related stress and strain in the pathophysiology of glaucomatous optic nerve head damage. *Prog Retin Eye Res*. 2005;24:39–73.
4. Hollander H, Makarov F, Stefani FH, Stone J. Evidence of constriction of optic nerve axons at the lamina cribrosa in the normotensive eye in humans and other mammals. *Ophthalmic Res*. 1995;27:296–309.
5. Morgan JE, Jeffery G, Foss AJ. Axon deviation in the human lamina cribrosa. *Br J Ophthalmol*. 1998;82:680–683.
6. Quigley HA, Addicks EM, Green WR, Maumenee AE. Optic nerve damage in human glaucoma. II. The site of injury and susceptibility to damage. *Arch Ophthalmol*. 1981;99:635–649.
7. Radius RL. Optic nerve fast axonal transport abnormalities in primates. Occurrence after short posterior ciliary artery occlusion. *Arch Ophthalmol*. 1980;98:2018–2022.
8. Radius RL. Regional specificity in anatomy at the lamina cribrosa. *Arch Ophthalmol*. 1981;99:478–480.
9. Radius RL, Bade B. Axonal transport interruption and anatomy at the lamina cribrosa. *Arch Ophthalmol*. 1982;100:1661–1664.
10. Anderson DR. Ultrastructure of human and monkey lamina cribrosa and optic nerve head. *Arch Ophthalmol*. 1969;82:800–814.
11. Burgoyne CF, Downs JC, Bellezza AJ, Hart RT. Three-dimensional reconstruction of normal and early glaucoma monkey optic nerve head connective tissues. *Invest Ophthalmol Vis Sci*. 2004;45:4388–4399.
12. Quigley HA, Addicks EM. Chronic experimental glaucoma in primates. II. Effect of extended intraocular pressure elevation on optic nerve head and axonal transport. *Invest Ophthalmol Vis Sci*. 1980;19:137–152.
13. Weinreb RN, Lindsey JD. The importance of models in glaucoma research. *J Glaucoma*. 2005;14:302–304.
14. Caprioli J, Ishii Y, Kwong JM. Retinal ganglion cell protection with geranylgeranylacetone, a heat shock protein inducer, in a rat glaucoma model. *Trans Am Ophthalmol Soc*. 2003;101:39–51.
15. Fortune B, Bui BV, Morrison JC, et al. Selective ganglion cell functional loss in rats with experimental glaucoma. *Invest Ophthalmol Vis Sci*. 2004;45:1854–1862.
16. Levkovitch-Verbin H, Quigley HA, Martin KR, et al. The transcription factor c-jun is activated in retinal ganglion cells in experimental rat glaucoma. *Exp Eye Res*. 2005;80:663–670.
17. Mittag TW, Danias J, Pohorenec G, et al. Retinal damage after 3 to 4 months of elevated intraocular pressure in a rat glaucoma model. *Invest Ophthalmol Vis Sci*. 2000;41:3451–3459.
18. Morrison JC. Elevated intraocular pressure and optic nerve injury models in the rat. *J Glaucoma*. 2005;14:315–317.

19. Neufeld AH, Sawada A, Becker B. Inhibition of nitric-oxide synthase 2 by aminoguanidine provides neuroprotection of retinal ganglion cells in a rat model of chronic glaucoma. *Proc Natl Acad Sci U S A*. 1999;96:9944–9948.
20. Quigley HA, McKinnon SJ, Zack DJ, et al. Retrograde axonal transport of BDNF in retinal ganglion cells is blocked by acute IOP elevation in rats. *Invest Ophthalmol Vis Sci*. 2000;41:3460–3466.
21. Aihara M, Lindsey JD, Weinreb RN. Experimental mouse ocular hypertension: establishment of the model. *Invest Ophthalmol Vis Sci*. 2003;44:4314–4320.
22. Grozdanic SD, Betts DM, Sakaguchi DS, Allbaugh RA, Kwon YH, Kardon RH. Laser-induced mouse model of chronic ocular hypertension. *Invest Ophthalmol Vis Sci*. 2003;44:4337–4346.
23. Libby RT, Anderson MG, Pang IH, et al. Inherited glaucoma in DBA/2J mice: pertinent disease features for studying the neurodegeneration. *Vis Neurosci*. 2005;22:637–648.
24. Mabuchi F, Aihara M, Mackey MR, Lindsey JD, Weinreb RN. Optic nerve damage in experimental mouse ocular hypertension. *Invest Ophthalmol Vis Sci*. 2003;44:4321–4330.
25. Howell GR, Libby RT, John SW. Mouse genetic models: an ideal system for understanding glaucomatous neurodegeneration and neuroprotection. *Prog Brain Res*. 2008;173:303–321.
26. John SW. Mechanistic insights into glaucoma provided by experimental genetics the cogan lecture. *Invest Ophthalmol Vis Sci*. 2005;46:2649–2661.
27. John SW, Anderson MG, Smith RS. Mouse genetics: a tool to help unlock the mechanisms of glaucoma. *J Glaucoma*. 1999;8:400–412.
28. Peters LL, Robledo RF, Bult CJ, Churchill GA, Paigen BJ, Svenson KL. The mouse as a model for human biology: a resource guide for complex trait analysis. *Nat Rev Genet*. 2007;8:58–69.
29. Whitmore AV, Libby RT, John SW. Glaucoma: thinking in new ways-a role for autonomous axonal self-destruction and other compartmentalised processes? *Prog Retin Eye Res*. 2005;24:639–662.
30. Morrison J, Farrell S, Johnson E, Deppmeier L, Moore CG, Grossmann E. Structure and composition of the rodent lamina cribrosa. *Exp Eye Res*. 1995;60:127–135.
31. May CA, Lutjen-Drecoll E. Morphology of the murine optic nerve. *Invest Ophthalmol Vis Sci*. 2002;43:2206–2212.
32. Campbell CB. Taxonomic status of tree shrews. *Science*. 1966;153:436.
33. Baldivia S, Levy A, Hegde S, Aper SJ, Merkx M, Grytz R. A novel organ culture model to quantify collagen remodeling in tree shrew sclera. *PLoS One*. 2016;11:e0166644.
34. Norton TT. Experimental myopia in tree shrews. *Ciba Found Symp*. 1990;155:178–194.
35. Albon J, Farrant S, Akhtar S, et al. Connective tissue structure of the tree shrew optic nerve and associated ageing changes. *Invest Ophthalmol Vis Sci*. 2007;48:2134–2144.
36. Samsel PA, Kisiswa L, Erichsen JT, Cross SD, Morgan JE. A novel method for the induction of experimental glaucoma using magnetic microspheres. *Invest Ophthalmol Vis Sci*. 2011;52:1671–1675.
37. Reynaud J, Cull G, Wang L, et al. Automated quantification of optic nerve axons in primate glaucomatous and normal eyes–method and comparison to semi-automated manual quantification. *Invest Ophthalmol Vis Sci*. 2012;53:2951–2959.
38. Janecka JE, Miller W, Pringle TH, et al. Molecular and genomic data identify the closest living relative of primates. *Science*. 2007;318:792–794.
39. Collins PM, Tsang WN, Metzger JM. Influence of stress on adrenocortical function in the male tree shrew (Tupaia belangeri). *Gen Comp Endocrinol*. 1984;55:450–457.
40. Walter E, Keist R, Niederost B, Pult I, Blum HE. Hepatitis B virus infection of tupaia hepatocytes in vitro and in vivo. *Hepatology*. 1996;24:1–5.
41. Urcola JH, Hernandez M, Vecino E. Three experimental glaucoma models in rats: comparison of the effects of intraocular pressure elevation on retinal ganglion cell size and death. *Exp Eye Res*. 2006;83:429–437.
42. Ervin JC, Lemij HG, Mills RP, Quigley HA, Thompson HW, Burgoyne CF. Clinician change detection viewing longitudinal stereophotographs compared to confocal scanning laser tomography in the LSU Experimental Glaucoma (LEG) Study. *Ophthalmology*. 2002;109:467–481.
43. Fortune B, Reynaud J, Hardin C, Wang L, Sigal IA, Burgoyne CF. Experimental glaucoma causes optic nerve head neural rim tissue compression: a potentially important mechanism of axon injury. *Invest Ophthalmol Vis Sci*. 2016;57:4403–4411.
44. Drenhaus U, von Gunten A, Rager G. Classes of axons and their distribution in the optic nerve of the tree shrew (*Tupaia belangeri*). *Anat Rec*. 1997;249:103–116.
45. Girkin CA, Fazio MA, Yang H, et al. Variation in the three-dimensional histomorphometry of the normal human optic nerve head with age and race: lamina cribrosa and peripapillary scleral thickness and position. *Invest Ophthalmol Vis Sci*. 2017;58:3759–3769.
46. Roberts MD, Grau V, Grimm J, et al. Remodeling of the connective tissue microarchitecture of the lamina cribrosa in early experimental glaucoma. *Invest Ophthalmol Vis Sci*. 2009;50:681–690.
47. Grau V, Downs JC, Burgoyne CF. Segmentation of trabeculated structures using an anisotropic Markov random field: application to the study of the optic nerve head in glaucoma. *IEEE Trans Med Imaging*. 2006;25:245–255.

Investigative Ophthalmology & Visual Science